Applied Physics Letters

An architecture for integrating planar and 3D cQED devices

C. Axline, M. Reagor, R. Heeres, P. Reinhold, C. Wang, K. Shain, W. Pfaff, Y. Chu, L. Frunzio, and R. J. Schoelkopf

View Online   Export Citation   CrossMark

ARTICLES YOU MAY BE INTERESTED IN

Reaching 10 ms single photon lifetimes for superconducting aluminum cavities
Applied Physics Letters **102**, 192604 (2013); https://doi.org/10.1063/1.4807015

Demonstration of superconducting micromachined cavities
Applied Physics Letters **107**, 192603 (2015); https://doi.org/10.1063/1.4935541

Surface participation and dielectric loss in superconducting qubits
Applied Physics Letters **107**, 162601 (2015); https://doi.org/10.1063/1.4934486

An architecture for integrating planar and 3D cQED devices

C. Axline, M. Reagor, R. Heeres, P. Reinhold, C. Wang, K. Shain, W. Pfaff, Y. Chu, L. Frunzio, and R. J. Schoelkopf
Department of Applied Physics, Yale University, New Haven, Connecticut 06511, USA

Numerous loss mechanisms can limit coherence and scalability of planar and 3D-based circuit quantum electrodynamics (cQED) devices, particularly due to their packaging. The low loss and natural isolation of 3D enclosures make them good candidates for coherent scaling. We introduce a coaxial transmission line device architecture with coherence similar to traditional 3D cQED systems. Measurements demonstrate well-controlled external and on-chip couplings, a spectrum absent of cross-talk or spurious modes, and excellent resonator and qubit lifetimes. We integrate a resonator-qubit system in this architecture with a seamless 3D cavity, and separately pattern a qubit, readout resonator, Purcell filter, and high-Q stripline resonator on a single chip. Device coherence and its ease of integration make this a promising tool for complex experiments. *Published by AIP Publishing.* [http://dx.doi.org/10.1063/1.4959241]

Superconducting quantum systems are becoming increasingly complex, with single packages incorporating on the order of ten coherent elements (resonators and qubits) used to store or process quantum information.[1] Tens of logical modules, or hundreds of elements, are needed to build systems capable of quantum error correction and operations with logical qubits.[2] As they scale, these larger systems must retain the level of control and coherence of smaller systems in order to achieve scalable levels of performance.

Planar architectures, patterned by lithography on a single substrate, are the basis for many circuit quantum electrodynamics (cQED) devices. Planar designs have several advantages: added complexity with little marginal effort, devices that can be consistently mass-produced, and sub-micrometer precision that offers good dimensional control over mode frequencies and coupling strengths. However, simple planar devices already face performance limits that may be further restricted by scaling. Losses, cross-talk, and package modes can be difficult to suppress given the presence of circuit board materials, wirebonds, isolated ground planes, and connectors.[3]

Device architectures based on 3D cavities also have distinct advantages. Large mode volumes and few loss-inducing elements can lead to exceptionally long cavity and qubit coherence times.[4–6] External coupling is easily adjusted over a large range, and the design provides a well-controlled spectrum of modes. Coupling (and any cross-talk) between adjacent enclosures can be made arbitrarily small. Just like planar circuits, however, 3D cavities can be susceptible to lossy package elements like seams.[7]

Proposals for scaled designs already consider some combination of planar and 3D structures.[8,9] We aim to create a platform for scaling in which many lithographically defined elements are combined within 3D enclosures, incorporating as many of the advantages discussed above as possible. By further integrating this design with the longest-lived 3D cavities available, the coherent complexity of this design could pave the way for error-correctable modules.[10,11]

In the following, we design and evaluate a carefully engineered 3D waveguide package for cQED devices. By enclosing planar circuit elements in this package, the resulting coaxial transmission line resonator-based ("coax-line") device can be highly coherent. Addressing a host of likely losses within the package, including coupling, seams, and materials, we observe single photon relaxation rates at the level of the state of the art ($\sim$50 μs) for planar elements. Resonators, qubits, and filters are fabricated together on a single chip. We demonstrate well-controlled coupling between them, set lithographically. Finally, we integrate this system with millisecond 3D "coax stub" cavities. In the near-term, this platform allows for significantly more complex many-resonator, many-qubit circuits. When combined with more advanced techniques for fabricating 3D enclosures using lithography and multi-wafer bonding,[9] the coax-line provides an attractive route towards long-term scaling.

To begin to demonstrate these combined advantages, we design and measure circuits placed in 3D enclosures. A seamless circular waveguide forms the package enclosure and acts as a ground plane (Figure 1(a)). Circuit elements are patterned on a sapphire substrate to define each mode of the device. Deposited and machined metals are both chosen to be aluminum. Where no metal is present on-chip, the waveguide attenuates signals below its cutoff frequency (typically 40 GHz). The chip is suspended within the enclosure by clamps at each end, where the fields from critical circuit elements are exponentially attenuated.

We evaluate device performance beginning with one simple element: a resonator. Choosing a quasi-stripline architecture, we pattern a $\lambda/2$ resonator on the substrate and position it near the center of the enclosure. The resonant frequency is primarily determined by the length of the conducting strip, but also depends on chip size, chip placement, and enclosure diameter.

Input and output signals are introduced using two evanescently coupled pins within sub-cutoff waveguides that intersect the primary waveguide enclosure. Pins are recessed to an adjustable depth within each coupling enclosure, located above each end of the stripline. Both pins are used in transmission measurements (Figure 1(b)). Just one pin can
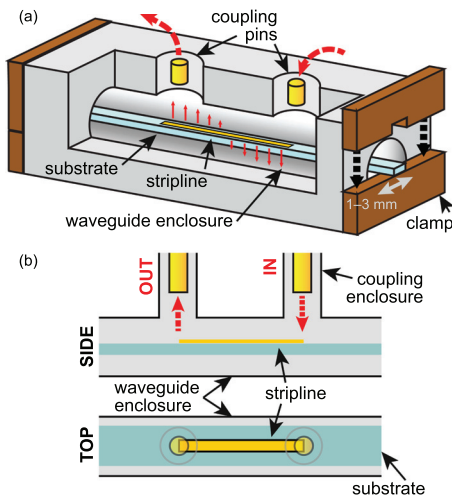
FIG. 1. (a) A depiction of the coax-line architecture includes a patterned sapphire chip (blue) inserted into a tubular enclosure and clamped at both ends (brown). Indium wire (not shown) secures the chip within the clamps. The resonator is patterned in the center of the chip, acting as the center conductor of a coaxial transmission line resonator. The enclosure ends are many attenuation lengths away from the resonator. Small red arrows represent the electric field pattern of the $\lambda/2$ resonant mode. Dashed arrows indicate the input and output paths used in transmission measurements. Coupling pins (gold), recessed within two smaller waveguides that intersect the primary enclosure, couple evanescently and carry signals to external connectors. (b) The configuration of couplers in a symmetric transmission experiment.

be used to measure in reflection or feedline-coupled transmission.[12] As described later, this approach yields predictable couplings that can be varied over a wide dynamic range without compromising package integrity.

To confirm that we retain the high coherence of 3D cavities, we evaluate resonator lifetimes. For resonators, this requires achieving a high internal quality factor (Q_i) at sufficiently weak coupling (high coupling quality factor Q_c). We measure these parameters by cooling coax-line resonators to $\sim$20 mK and exciting single-photon-or-less circulating power. The devices are connected in a feedline-coupled configuration and the transmission coefficient S_{21} is measured using a vector network analyzer (VNA). Coupling parameters are extracted from fits to S_{21} (Figure 2(a) inset). Measurements are usually performed in an undercoupled configuration

($Q_c \geq Q_i$, with Q_c up to 10^9) so that the total quality factor Q ($1/Q = 1/Q_i + 1/Q_c$) is a direct measure of the internal losses. The best reported Q_i for lithographically defined aluminum-on-sapphire resonators fabricated under similar conditions (e-beam evaporation, no substrate annealing) is $\sim$$1 \times 10^6$.[13] We observe Q_i as high as $(8.0\pm0.5) \times 10^6$ at single-photon power, surpassing this by about an order of magnitude. This suggests that quality factors in lithographic devices are not solely dependent on materials or fabrication methods, but are also affected by package contributions.

By restricting wave propagation to seamless waveguides with cutoffs far above the operating frequency, we demonstrate that mode coupling can be made arbitrarily weak without additional structures or filtering.[14] This implements the robust coupling method used in 3D cavities. By varying the coupling attenuation distance and measuring Q_c, we see good agreement with the expected exponential scaling over six decades with no observed upper limit (Figure 2(b)). Control over a large dynamic range in coupling strengths is possible by simply modifying pin length. Therefore, we can achieve very strong coupling ($Q_c \sim 10^3$) to some elements used for measurement or readout, at the same time as weak couplings ($Q_c \sim 10^8$) used to excite and control long-lived memory elements.

Another critical requirement of a properly designed package, and a property inherent to 3D cavities, is the prevention of spurious electromagnetic modes. Using stronger coupling and a symmetric transmission configuration, we measured S_{21} to determine the spectral "cleanliness" over a large range. Because the enclosure should attenuate any modes below its cutoff frequency in the absence of package seams, we expect the measured background to be low, dominated by the noise of other elements in the measurement chain. Figure 2(c) shows a calibrated S_{21} trace within the measurement bandwidth of our high electron mobility transistor (HEMT) amplifier. Aside from the fundamental ($\lambda/2$) and first harmonic (λ) modes arising from the stripline resonator, no other modes are observed. This confirms that good mode control can be achieved using a coax-line architecture.

As the next step in increasing complexity—a characteristic of planar devices that we aimed to implement—we
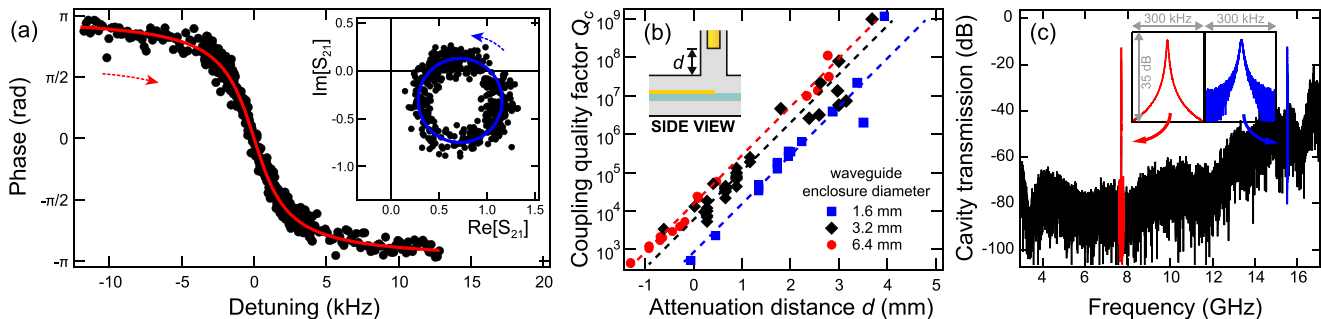

FIG. 2. (a) Resonator quality factors Q_i and Q_c are extracted from fits of the resonance circle in S_{21} (inset) and the phase response (main figure).[15] Data are measured at an average cavity photon number $\bar{n} \approx 1$ where unsaturated defects produce 30%–50% lower Q relative to higher powers.[16] A representative sample, plotted, has $Q_i = (5.98 \pm 0.07) \times 10^6$ and $Q_c = (4.27 \pm 0.07) \times 10^6$. Dashed arrows indicate frequency sweep direction. (b) Coupling quality factor Q_c is measured for 12 mm-long resonators in enclosures with three different diameters (solid points). The attenuation distance d (inset) is measured from the end of the coupling pin to the edge of the enclosure, and enters the enclosure for $d < 0$. We measure Q_c as high as 10^9, above which reduced SNR hinders measurement for our typical Q_i's. Measured Q_c's follow exponential behavior (dashed lines) with minor deviations due to resonator shape, chip placement, and machining variance. This suggests that no unknown mode couples more strongly than $Q_c = 10^9$. (c) Transmission measurements ($20 \log |S_{21}|$) show only the expected resonant modes, here at 7.7 GHz and 15.5 GHz. The fundamental mode sees isolation of $>$60 dB. The noise floor is due to the frequency dependence of the readout system and HEMT noise.

pattern a transmon qubit alongside the resonator.[17] We characterize the system's coherence and compare measured parameters to simulation. We control the qubit using a weakly coupled port and read out through the resonator and its more strongly coupled port. These qubits exhibit 30–80 μs lifetimes, near to the state of the art values for transmon T_1's (Figure 3(a)). This is equivalent to quality factors $\leq 3 \times 10^6$, not far from those of resonators. Undercoupled resonators had equally high Q_i with and without qubits. Important system parameters, such as mode frequencies and qubit anharmonicity, were found to agree well with predictions from finite-element simulations of the design.[12,18] This is the first indication that additional complexity can be added to a coax-line device without decreasing control over parameters or coherence values.

The presence of a lithographic resonator-qubit system enables us to test whether on-chip element coupling follows the same waveguide-attenuated behavior as external coupling. We expect that by varying the distance z between element ends (Figure 3(b) inset), the chip enclosure will exponentially attenuate electric field $|\vec{E}| \propto e^{-\alpha z}$. The resonator-qubit dispersive shift χ should scale as $\chi \sim |\vec{E}|^2$. However, different resonator-qubit detunings Δ between samples make direct comparison difficult. To relate them consistently to z, we calculate an effective coupling g defined by the relation $\chi = 2g^2/\Delta$, related to the detuned Jaynes-Cummings model.[19] When z is varied experimentally, we find that the measured change in g is consistent with a calculated waveguide attenuation scale length $1/\alpha \approx 1.02$ mm, as well as with simulations (Figure 3(b)). This suggests that no unintended coupling is present and that reasonably small separations between elements can produce a range of qubit-resonator couplings useful for typical cQED applications. Furthermore, we demonstrate another advantage typical of planar devices: tight dimensional and coupling control.

The lifetimes of resonators and qubits in this system can be understood by examining the spatial participation of each mode in dissipative dielectrics and conductors. The large resonator mode volume dilutes lossy material participation—the same effect that increases coherence of 3D cavities relative to traditional planar circuits. By measuring resonators in

waveguide enclosures with different diameters, we find that higher Q_i generally corresponds with larger diameter.[12] This scaling behavior is consistent with loss originating from waveguide surface resistance, a waveguide dielectric layer, or on-chip dielectric layers, but does not distinguish between these mechanisms.

Even though the enclosure body is seam-free, we can evaluate whether seams at each end introduce dissipation. We predict their effect using a model of seam loss as a distributed admittance[7] applied to simulation. The simulation places a conservative bound, $Q_i \geq 10^8$, on typical designs separated 7 mm from the waveguide end. Positioning striplines $\sim$3 mm from one end of an enclosure produced an immeasurable effect on Q_i, thereby raising this bound. Since typical devices see significantly greater isolation from end seams, they appear unlikely to affect performance. Therefore, coax-line devices are well-positioned to act as a testbed for alternative loss mechanisms. Further studies will be required to pinpoint the dominant sources of loss, but the coherence levels already achieved allow us to increase the system's complexity further.

Many circuit elements must be integrated within a single enclosure to allow more versatile, hardware-efficient cQED experiments. To demonstrate an instance of a long-lived element in the presence of significant complexity, we combine a very high-Q 3D cavity with the coax-line architecture. In the resulting package (Figure 4(a)), the pads of a transmon qubit bridge two structures: the coax-line qubit-and-stripline system and a 3D coaxial stub cavity.[6]

We characterize parameters of the complete system, including coupling and coherence values. Both the qubit and the high-Q cavity perform well (qubit $T_1 = 110\,\mu$s; qubit Ramsey decay time $T_2^* = 40\,\mu$s; cavity $T_1 = 2.8$ ms, Figure 4(b); cavity $T_2^* = 1.5$ ms for the $|0\rangle + |1\rangle$ Fock state superposition[6]). These qubit lifetimes are among the best measured in 3D cavities, and the coaxial stub resonator T_1 does not decrease when a qubit is added. This suggests that no additional sources of dissipation are introduced when these elements are combined into a single, seamless package.

Integration with 3D cavities is not strictly necessary to produce a module with many coherent circuit elements. In an all-lithographic system on a single chip, we can add
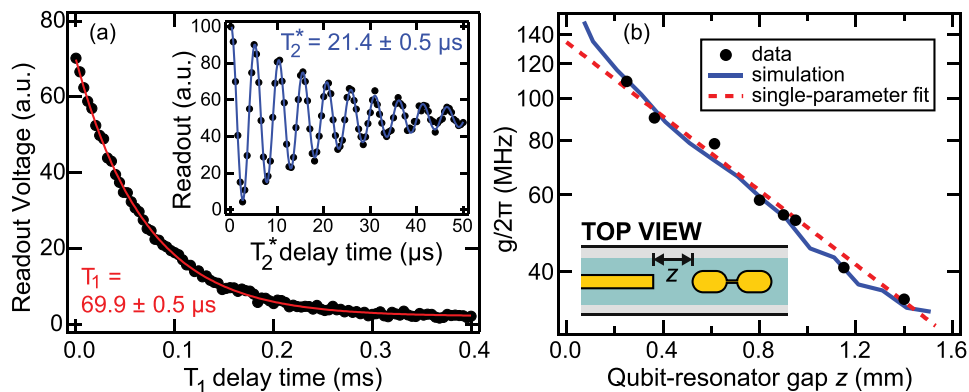

FIG. 3. A qubit is placed adjacent to a stripline resonator (Figure 1(b)). (a) Qubit T_1 (main figure) and T_2^* (inset) of one characteristic device. The T_1 experiment is fit to an exponential (red), while the detuned T_2^* Ramsey experiment is fit to an exponentially decaying sine function (blue). (b) Coupling between the qubit and stripline resonator is controlled by adjusting their end-to-end separation z (inset). Values of effective qubit-stripline coupling rate g are measured for different z (black points) and fit using an exponential function $Ae^{-\alpha z}$ (dashed red line) with single free parameter A. The calculated attenuation, 8.5 dB/mm, comes from simulation of a 2.8 mm-diameter waveguide with bare substrate. A full system finite-element simulation (solid blue line) predicts similar scaling.
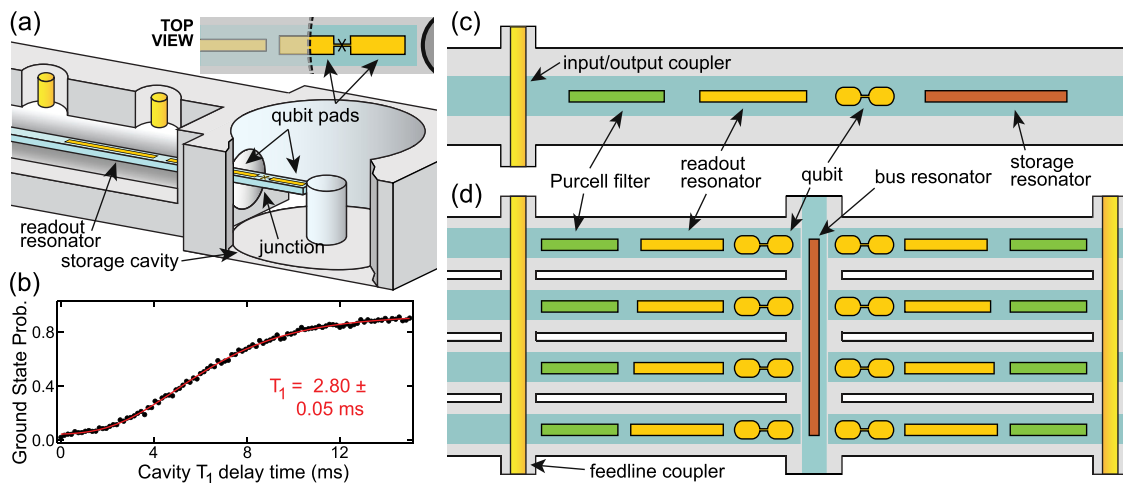
FIG. 4. (a) Combining a chip-based circuit with a 3D coaxial stub cavity. The transmon qubit antenna pads straddle the circular waveguide enclosure and stub cavity. Qubit-stripline coupling is controlled lithographically, and qubit-cavity coupling is set by antenna geometry and chip position. (b) Cavity T_1 is fit (red) to data (black points). The cavity lifetime is not spoiled by the qubit's shorter lifetime. (c) We extended the chip-based qubit-stripline system by adding a Purcell filter and high-Q stripline storage resonator. It requires a single pin-coupler in a feedline-coupled configuration. (d) We propose an expansion of multiple chip-based modules, in which eight Purcell-filtered qubits interact with a bus resonator and are addressed by two multiplexed readout lines.

components without sacrificing the isolation between non-adjacent elements. Figure 4(c) shows a coax-line variant with two additional stripline resonators. These resonators function as a bandpass Purcell filter[20,21] and high-Q storage resonator. We measure coherence consistent with qubit-and-stripline designs (best qubit $T_1 \approx 60\,\mu s$, $T_2^* \approx 50\,\mu s$, and Hahn echo decay time $T_2 \approx 60\,\mu s$) and with a large cavity decay rate and qubit-readout coupling. Numerous devices were measured, producing consistently long lifetimes (Table S2 in the supplementary materials[12]). The best stripline storage resonator in this four-element module has $T_1 = 250\,\mu s$, or an equivalent $Q_i = 11.2 \times 10^6$. These results demonstrate that entirely chip-based designs can produce a highly coherent quantum module. A concept for how these modules could be expanded, including eight Purcell-filtered qubits and two multiplexed readout lines, is shown in Figure 4(d).

We have introduced a 3D enclosure and chip-based coax-line architecture that allows for complex cQED experiments. The device construction, absent of seams and based on natural waveguide isolation, suppresses spurious modes and allows for precisely engineered couplings. Using under-coupled stripline resonators, we measured the highest Q_i in a chip-based cQED device to date. We integrated this type of resonator with a qubit and a millisecond 3D cavity without introducing further loss, creating a long-lived, multi-cavity cQED system. This implementation combines advantages of planar systems (complexity, dimensional control) and 3D systems (coherence, coupling, and spectral cleanliness), and suffers little from mechanical assembly uncertainty.[12] Adaptations of this system have already been used in more complex experiments with multiple qubits or cavities.[22,23]

This architecture could enable useful capabilities in future designs. On-chip amplification schemes could possibly be integrated with readout feedlines, allowing multiplexed single-shot readout. Many more elements could be added, producing dense multi-qubit, multi-cavity systems. The concept could apply to wafer-scale micromachining

designs, where more complex, multi-layer circuits could be fabricated.[9]

This flexibility, in addition to high coherence properties, may yet inspire the next generation of hardware towards fault-tolerant error correction.

[1]R. Barends, J. Kelly, A. Megrant, A. Veitia, D. Sank, E. Jeffrey, T. C. White, J. Mutus, A. G. Fowler, B. Campbell, Y. Chen, Z. Chen, B. Chiaro, A. Dunsworth, C. Neill, P. O'Malley, P. Roushan, A. Vainsencher, J. Wenner, A. N. Korotkov, A. N. Cleland, and J. M. Martinis, Nature **508**, 500 (2014).
[2]A. M. Steane, Phys. Rev. A **68**, 042322 (2003).
[3]Z. Chen, A. Megrant, J. Kelly, R. Barends, J. Bochmann, Y. Chen, B. Chiaro, A. Dunsworth, E. Jeffrey, J. Y. Mutus, P. J. J. O'Malley, C. Neill, P. Roushan, D. Sank, A. Vainsencher, J. Wenner, T. C. White, A. N. Cleland, and J. M. Martinis, Appl. Phys. Lett. **104**, 052602 (2014).
[4]H. Paik, D. I. Schuster, L. S. Bishop, G. Kirchmair, G. Catelani, A. P. Sears, B. R. Johnson, M. J. Reagor, L. Frunzio, L. I. Glazman, S. M. Girvin, M. H. Devoret, and R. J. Schoelkopf, Phys. Rev. Lett. **107**, 240501 (2011).
[5]O. Dial, D. T. McClure, S. Poletto, G. A. Keefe, M. B. Rothwell, J. M. Gambetta, D. W. Abraham, J. M. Chow, and M. Steffen, Superconductor Science and Technology **29**, 044001 (2016).
[6]M. Reagor, W. Pfaff, C. Axline, R. W. Heeres, N. Ofek, K. Sliwa, E. Holland, C. Wang, J. Blumoff, K. Chou, M. J. Hatridge, L. Frunzio, M. H. Devoret, L. Jiang, and R. J. Schoelkopf, Phys. Rev. B **94**, 014506 (2016).

[7]T. Brecht, M. Reagor, Y. Chu, W. Pfaff, C. Wang, L. Frunzio, M. H. Devoret, and R. J. Schoelkopf, Appl. Phys. Lett. **107**, 192603 (2015).

[8]J. M. Gambetta, J. M. Chow, and M. Steffen, e-print arXiv:1510.04375 [quant-ph].

[9]T. Brecht, W. Pfaff, C. Wang, Y. Chu, L. Frunzio, M. H. Devoret, and R. J. Schoelkopf, npj Quantum Inf. **2**, 16002 (2016).

[10]M. H. Devoret and R. J. Schoelkopf, Science **339**, 1169 (2013).

[11]N. H. Nickerson, J. F. Fitzsimons, and S. C. Benjamin, Phys. Rev. X **4**, 041041 (2014).

[12]See supplementary material at http://dx.doi.org/10.1063/1.4959241 for experimental details.

[13]A. Megrant, C. Neill, R. Barends, B. Chiaro, Y. Chen, L. Feigl, J. Kelly, E. Lucero, M. Mariantoni, P. J. J. O'Malley, D. Sank, A. Vainsencher, J. Wenner, T. C. White, Y. Yin, J. Zhao, C. J. Palmstrøm, J. M. Martinis, and A. N. Cleland, Appl. Phys. Lett. **100**, 113510 (2012).

[14]M. Sandberg, M. R. Vissers, T. A. Ohki, J. Gao, J. Aumentado, M. Weides, and D. P. Pappas, Appl. Phys. Lett. **102**, 072601 (2013).

[15]M. S. Khalil, M. J. A. Stoutimore, F. C. Wellstood, and K. D. Osborn, J. Appl. Phys. **111**, 054510 (2012).

[16]J. Gao, M. Daal, A. Vayonakis, S. Kumar, J. Zmuidzinas, B. Sadoulet, B. A. Mazin, P. K. Day, and H. G. Leduc, Appl. Phys. Lett. **92**, 152505 (2008).

[17]M. Devoret, S. Girvin, and R. Schoelkopf, Ann. Phys. **16**, 767 (2007).

[18]S. E. Nigg, H. Paik, B. Vlastakis, G. Kirchmair, S. Shankar, L. Frunzio, M. H. Devoret, R. J. Schoelkopf, and S. M. Girvin, Phys. Rev. Lett. **108**, 240502 (2012).

[19]A. Wallraff, D. I. Schuster, A. Blais, L. Frunzio, R.-S. Huang, J. Majer, S. Kumar, S. M. Girvin, and R. J. Schoelkopf, Nature **431**, 162 (2004).

[20]M. D. Reed, B. R. Johnson, A. A. Houck, L. DiCarlo, J. M. Chow, D. I. Schuster, L. Frunzio, and R. J. Schoelkopf, Appl. Phys. Lett. **96**, 203110 (2010).

[21]E. Jeffrey, D. Sank, J. Mutus, T. White, J. Kelly, R. Barends, Y. Chen, Z. Chen, B. Chiaro, A. Dunsworth, A. Megrant, P. O'Malley, C. Neill, P. Roushan, A. Vainsencher, J. Wenner, A. Cleland, and J. M. Martinis, Phys. Rev. Lett. **112**, 190504 (2014).

[22]J. Z. Blumoff, K. Chou, C. Shen, M. Reagor, C. Axline, R. T. Brierley, M. P. Silveri, C. Wang, B. Vlastakis, S. E. Nigg, L. Frunzio, M. H. Devoret, L. Jiang, S. M. Girvin, and R. J. Schoelkopf, e-print arXiv:1606.00817 [quant-ph].

[23]C. Wang, Y. Y. Gao, P. Reinhold, R. W. Heeres, N. Ofek, K. Chou, C. Axline, M. Reagor, J. Blumoff, K. M. Sliwa, L. Frunzio, S. M. Girvin, L. Jiang, M. Mirrahimi, M. H. Devoret, and R. J. Schoelkopf, Science **352**, 1087 (2016).